Journal of Hydrology 567 (2018) 351–360

Contents lists available at ScienceDirect

Journal of Hydrology

journal homepage: www.elsevier.com/locate/jhydrol

Research papers

Role of mudflat-creek sediment exchanges in intertidal sedimentary processes

Weiming Xie[a,b], Qing He[a,*], Xianye Wang[a], Leicheng Guo[a], Keqi Zhang[c,d]

[a] State Key Laboratory of Estuarine and Coastal Research, East China Normal University, Shanghai 200062, China
[b] Yellow River Institute of Hydraulic Research, Yellow River Conservancy Commission, Zhengzhou 450003, China
[c] Department of Earth and Environment, Florida International University, Miami, FL 33199, USA
[d] International Hurricane Research Center, Florida International University, Miami, FL 33199, USA

ARTICLE INFO

This manuscript was handled by Andras Bardossy, Editor-in-Chief, with the assistance of Geoff Syme, Associate Editor

Keywords:
Intertidal environment
Mudflat-creek system
Hydrodynamics
Sedimentary process
Bed shear stress
Yangtze Estuary

ABSTRACT

Intertidal environments, including bare mudflats, tidal creeks, and vegetated salt marshes, are of significant physical and ecological importance in estuaries. Their morphodynamics are closely linked by mudflats and creek networks. Understanding water motion and sediment transport in mudflats and tidal creeks is fundamental to understand intertidal morphodynamics in intertidal environments. To explore dynamic interactions between tidal creeks and mudflats, we conducted field campaigns monitoring water depths, tidal currents, waves, suspended sediments, and bed-level changes at sites in both mudflats and tidal creeks in the Eastern Chongming tidal wetland in the Yangtze Delta for a full spring-neap tidal cycle. We saw that under fair weather conditions, the bed-level changes of the tidal creek site displayed a contrary trend compared with those of the mudflat site, indicating the source-sink relationship between tidal creek and mudflat. During over-marsh tides, the tidal creek site with relatively high bed shear stresses (averagely, 0.37 N/m^2) was eroded by 35 mm whereas the mudflat site was accreted by 29 mm under low bed shear stresses (averagely, 0.18 N/m^2). To the contrast, during creek-restricted tides, deposition occurred in the tidal creek site by 20 mm under low bed shear stresses (averagely, 0.09 N/m^2) whereas erosion occurred in the mudflat site by 25 mm under relatively high bed shear stresses (averagely, 0.21 N/m^2). Over a spring-neap tidal cycle, the net bed level changes were −15 mm (erosion) and 4 mm (deposition) in tidal creeks and mudflats, respectively. These results suggested that there were alternated erosion-deposition patterns in spring and neap tides, and a sediment source and sink shift between mudflats and creeks. We found that the eroded sediments in mudflats were transported landward into tidal creeks and deposited therein in neap tides, and these newly deposited sediments would be resuspended and transported to surrounding marshes (over-marsh deposition) at spring tides. The coherent sediment transport and associated erosion-deposition pattern within the mudflat-creek system at spring-neap tidal time scales thus played a fundamental role in intertidal morphodynamic development. These findings suggest that management and restoration of intertidal ecosystem need to take the entire mudflat-creek-marsh system as a unit into consideration rather than focusing on single elements.

1. Introduction

Intertidal environments are important elements in estuarine and coastal systems, supporting the exchange of materials like sediments and nutrients between the land and the ocean (Eisma, 1998; Nyman et al., 2009; Kirwan and Megonigal, 2013). Different types of ecosystems, like mudflats, salt marshes, and tidal creeks can be found within the intertidal fringe. Many previous studies have focused on the recognition of the valuable functions of these ecosystems, like providing coastal protection by dissipating waves, and defending from storm surges (Moller et al., 1999; Gedan et al., 2011; Temmerman et al., 2013), and providing ecological services by hosting migratory birds and feeding coastal benthos (Ysebaert et al., 2003; Tian et al., 2008). However, different coastal settings throughout the world such as the Scheldt Estuary, the Chesapeake Bay, the Venice Lagoon, the Bay of Fundy, and the Yangtze Estuary, are presently facing the loss of intertidal habitats as a result of combined effects of land reclamation, sea-level rise, and sediment supply reduction etc. (Temmerman et al., 2003; Yang et al., 2005; van Proosdij et al., 2006; D'Alpaos et al., 2007; Mariotti et al., 2010; Tian et al., 2015). In response, remarkable

* Corresponding author.
E-mail address: qinghe@sklec.ecnu.edu.cn (Q. He).

https://doi.org/10.1016/j.jhydrol.2018.10.027
Received 15 July 2018; Received in revised form 30 September 2018; Accepted 12 October 2018
Available online 14 October 2018

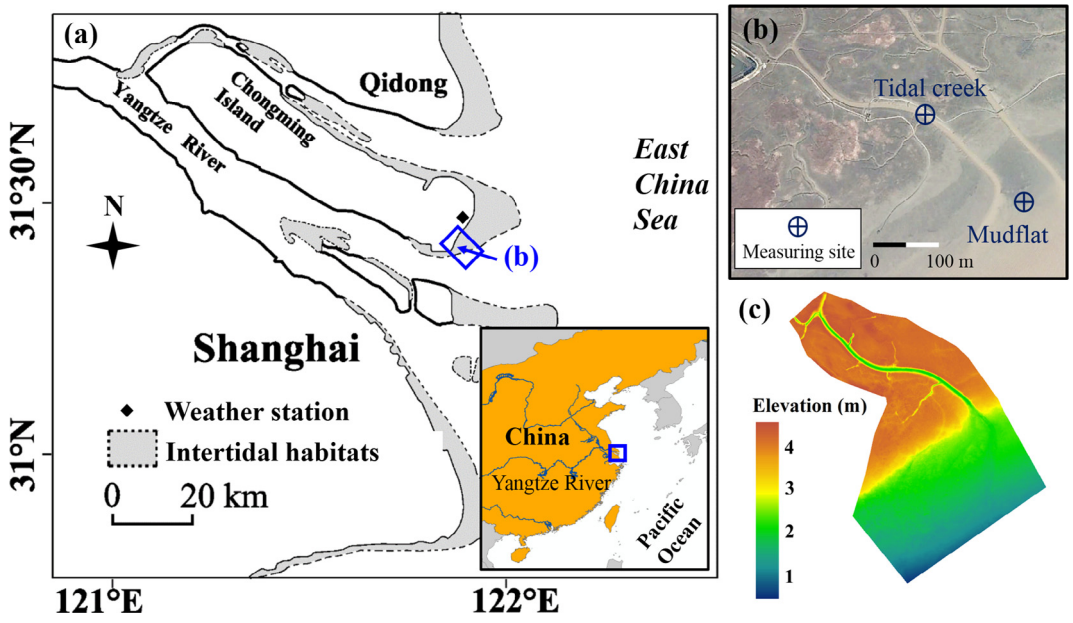

Fig. 1. Map of the Yangtze Estuary, location of Eastern Chongming weather station (a) and a view of the study site and locations of the two measuring sites (b), and Digital elevation model of the study area derived from Terrestrial Laser Scanning data collected in August 2016 (c).

changes would occur in terms of hydrodynamics and sedimentary processes within intertidal systems. Knowledge regarding the distribution and dynamics of flows and sediments is essential to advance understanding of morphological and ecological changes in intertidal environments.

Many researchers have monitored flow and sediment transported processes over intertidal environments and found that there were great differences in hydrodynamics and sedimentary processes between mudflats, tidal creeks, and salt marshes (Eisma, 1998; Dyer et al., 2000; Yang et al., 2003; Friedrichs, 2011; O'Laughlin and van Proosdij, 2013; Bouma et al., 2016; Eaton, 2016). Unvegetated mudflats, with lower elevations compared to salt marshes, can be submerged more frequently for longer time. A few theories highlight the dominance of tidal asymmetry and scour-and-settling-lag in controlling tide-averaged sediment transport and consequent morphological changes in mudflats (Postma, 1961; Dronkers, 1986; Wang et al., 2002). Based on those results, previous studies conclude that mudflat profiles can reach approximate dynamic equilibria with their local climate of waves, tides, and sediment sources when considered as an average over annual and longer timescales (Friedrichs, 2011; Hu et al., 2015; van der Wegen et al., 2017). Moreover, recent studies propose that erosion-deposition patterns of mudflats are actually governed by non-linear interactions between both tidal currents and wind waves (Janssen-Stelder, 2000; Widdows et al., 2008; Shi et al., 2012; Hunt et al., 2015). Sedimentary processes in the mudflats can be effectively predicted based on two parameters: bed shear stress derived from combined wave-current action (τ_{cw}) and critical bed shear stress for erosion (τ_{ce}) (Shi et al., 2012, 2017; Zhu et al., 2014).

Compared to the mudflats, sedimentary processes in the vegetated salt marshes are more complex and are determined by water motion, sediment transport, vegetation and elevation. Vegetation over the marshes could attenuate waves and stabilize sediment bed, which greatly reduces the combined wave-current shear stress (τ_{cw}) while enhances critical bed shear stress for erosion (τ_{ce}), respectively (Stumpf, 1983; Bouma et al., 2009; Howes et al., 2010; Vandenbruwaene et al., 2015). As a result, sediment deposition is more likely to occur than erosion in the salt marshes except for extremely high storm surges along with severe wave activities (Temmerman et al., 2005b; D'Alpaos et al., 2007; Fagherazzi and Wiberg, 2009; Howes et al., 2010; Leonardi et al., 2016). The elevation of marsh surface also plays an important role in sedimentary processes in the salt marshes. Except low marshes, most of salt marshes with a higher elevation are only submerged during high tides, thus only over-marsh tides are effective in controlling the sedimentary processes. Temmerman et al. (2003) also concludes that sedimentation rate of the salt marsh generally decreases with increasing surface elevation and distance from the nearest creek or marsh edge.

Tidal creeks are ubiquitous components of intertidal environments, flooding and draining the marsh platform, and providing conduits for sediments and nutrients to the marsh system (Voulgaris and Meyers, 2004; Fagherazzi et al., 2012; Xin et al., 2012). Previous studies have acknowledged that the tidal creek is the dominant supplier of sediment to the marsh surface, particularly for meso-tidal and micro-tidal regions (Allen, 2000; Friedrichs, 2011; O'Laughlin and van Proosdij, 2013). The tidal current and topography govern the flow magnitude, which influences the sedimentary processes in tidal creeks (D'Alpaos et al., 2007; O'Laughlin and van Proosdij, 2013). Numerical models and field measurements suggest that mudflats, salt marshes, and tidal creeks can significantly affect each other (Friedrichs, 2011; Fagherazzi et al., 2012; Schuerch et al., 2014). For instance, short-term mudflat dynamics can initiate adjacent lateral marsh erosion (Bouma et al., 2016). Hence, a combined study of the hydrodynamics and sediment transport in the three components is fundamental to understand the sedimentary processes when taking an intertidal environment as a whole into account. Recent studies focus on the interactions between tidal creeks and salt marshes (Temmerman et al., 2007; Mariotti and Fagherazzi, 2013), and interactions between salt marshes and mudflats (Bouma et al., 2016). However, there is insufficient knowledge of the interchanges between tidal creeks and mudflats. Specifically, it is poorly known: (1) how mudflats and tidal creeks influence each other through water motion and sediment transport, and (2) the role of the mudflat-creek system in the sedimentary processes for the entire intertidal environment.

This study is devoted to understanding sedimentary processes in a mudflat-creek system based on an integrated observation of currents, waves, sediments and bed-level changes in an intertidal habitat in the Yangtze Estuary. We aim to figure out intertidal morphodynamic behaviors between tidal creeks and mudflats, and the role of the mudflat-creek system in the morphodynamics of intertidal environments.

2. Methods

2.1. Study area

Field observations were conducted in the intertidal area of the Eastern Chongming Island, a 170 km^2 tidal wetland in the Yangtze Estuary (Fig. 1) (Li et al., 2014). Salt marshes, mudflats, and tidal creeks dominate a large portion of the intertidal zone. The tides in the Yangtze Estuary are dominantly semi-diurnal and the local mean tidal range is 2.5 m with maximum spring tidal range up to 5 m (Yang et al., 2008; Shi et al., 2012; Zhu et al., 2016). Monthly averaged wind velocity varies between 3.5 and 4.5 m/s and wave height in the intertidal environments normally ranges from 0.1 to 0.3 m and seldom exceeds 1.0 m even under severe stormy weather (Yang et al., 2008). The Eastern Chongming tidal wetland used to prograde seaward at an average rate of ~10 m/year, and the maximum rate was up to 226 m/year (Yang et al., 2001). Deposition of river-supplied sediment and extensive reclamation stimulate the growth of the tidal wetland. However, the accretion rate has strongly reduced in recent years due to the decrease of the Yangtze River supplied sediment, i.e., from 455 million tons per year in 1950–2000 to 150 million tons in 2001–2012 (van Maren et al., 2013; Luan et al., 2016; Wang et al., 2016).

Facing the East China Sea, the study site was located at the southern part of the Eastern Chongming tidal wetland, including mudflats, salt marshes and a tidal creek (Fig. 1b). The width of the tidal creek ranged from 30 m at the creek mouth to 2 m at the creek head, and the creek depth ranged from 2.5 to 0.5 m. The axial bed slope of the mudflat and tidal creek is 3‰ and 1.8‰, respectively. The surficial sediments are composed of clay and silt with median diameters smaller than 60 μm in the study area. The salt marsh surface and the upper creek banks were mainly vegetated by *Carex scabrifolia*.

2.2. Field measurements

Two hydrodynamic measurements were performed in the mudflat (100 m seaward from the marsh edge) and in the tidal creek (120 m landward from the creek mouth), respectively (Figs. 1b and 2a). Observations were conducted from 20:00 on August 2 to 10:00 on August 12, 2016, during a spring-neap tidal cycle covering 19 semi-diurnal tides. Hourly wind speeds and directions were recorded by the Eastern Chongming weather station, 4 km to the north of the study site (Fig. 1a). Current velocity, suspended sediment concentration (SSC), wave height, and bed-level change were monitored by two tripods mounted at the tidal creek site and the mudflat site (Fig. 2). The tripod was equipped with an Acoustic Doppler Velocimeter (ADV) (Nortek AS, Norway), Argus Surface Meter (ASM) (ARGUS, Germany), and RBR Tide & Wave Loggers (RBR) (RBR Limited, Canada). At the tidal creek site, the ADV, ASM, and RBR were placed 25, 25, and 7 cm above the bed surface, respectively, while they were placed 35, 35, and 5 cm, respectively, above the bed surface at the mudflat site. The ADV which was set up in the 64 Hz mode with a burst interval of 10 min, recorded the near-bed 3D velocity and bed-level change (Andersen et al., 2007; Salehi and Strom, 2012; Zhu et al., 2016). The RBR, sampling 512 bursts every 5 min at 4 Hz, were deployed to measure the wave activity and water depth. The optical backscatter signal of the ASM was used to estimate the SSC, sampling 25 bursts every 5 min. Calibration of the optical backscatter signal into SSC was shown in Fig. 2b.

The bed elevation of the study area was collected by Terrestrial Laser Scanner Riegl VZ4000 (Riegl, Austria) (Xie et al., 2017), relative to the theoretical low-tide datum at Wusong (Fig. 1c). The elevations of the tidal creek site and the mudflat site were 2.2 and 2.1 m above the datum, respectively (Fig. 2c and d). Bankfull elevations varied from 4.5 m in the high marsh to 4.2 m in the low marsh (Fig. 2c).

2.3. Estimation of bed shear stress

At the tidal creek site, the bed shear stress due to the current (τ_c) was dominant because of very small waves detected therein (Fig. 3). While at the mudflat site, the wave activities appeared stronger and more frequent. The bed shear stress derived from combined wave-current action (τ_{cw}) was essential for studying the mudflat morphodynamics (Shi et al., 2012; Zhu et al., 2014).

The 3D velocity derived from the ADV (*u, v, w*) can be decomposed into two terms: the mean (*U, V, W*) and turbulent components (*u′, v′, w′*). The turbulent kinetic energy (TKE) (J/m^3) and current-induced bed shear stress (τ_c) are calculated using:

$$TKE = \frac{1}{2}\rho(u'^2 + v'^2 + w'^2) \tag{1}$$

$$\tau_c = C \times TKE \tag{2}$$

where ρ is water density at 20 °C ($\rho = 1025\ kg/m^3$) (Voulgaris and Meyers, 2004; Andersen et al., 2007), and *C* is a constant ($C = 0.19$) (Stapleton and Huntley, 1995; Kim et al., 2000; Pope et al., 2006).

The bed shear stress due to waves (τ_w) is generally obtained from the wave orbital velocity U_δ(m/s) and wave friction coefficient f_w (Rijn, 1993):

$$\tau_w = \frac{1}{4}\rho_w f_w U_\delta \tag{3}$$

where ρ_w is the seawater density ($\rho_w = 1030\ kg/m^3$). The peak orbital excursion (A_δ) and (U_δ) can be expressed as (Zhu et al., 2016):

$$A_\delta = \frac{H}{2sinh(kh)} \tag{4}$$

$$U_\delta = \omega A_\delta = \frac{\pi H}{Tsinh(kh)} \tag{5}$$

where *H* is wave height (m), *T* is wave period (s), *h* is water depth (m), *k* is the wave number ($k = 2\pi/L$), ω is angular velocity (s^{-1}), *L* is the wavelength (m) ($L = (gT^2/2\pi)tanh(kh)$), and *g* is gravitational acceleration ($g = 9.8\ m/s^2$). The wave fiction coefficient depends on the hydraulic regime (Soulsby, 1997; Zhu et al., 2016):

$$f_w \begin{cases} 2Re_w^{-0.5},\ Re_w \le 10^5 (laminar) \\ 0.0521Re_w^{-0.187},\ Re_w > 10^5 (smooth\ \ turbulent) \\ 0.237r^{-0.52},\ (rough\ \ turbulent) \end{cases} \tag{6}$$

where $Re_w = \frac{U_\delta A_\delta}{\nu}$ and $r = \frac{A_\delta}{k_s}$ are the wave Reynolds number and relative roughness. k_s is the Nikuradse roughness expressed as $k_s = 2.5d_{50}$, where d_{50} is the median grain size of the bed sediment and ν is the kinematic viscosity of water ($\nu = 1.5 \times 10^{-6}\ m^2/s$).

The bed shear stress due to combined wave-current action (τ_{cw}) can be calculated from a hydrodynamic formulation (Soulsby, 1995; Shi et al., 2017):

$$\tau_{cw} = \tau_c \left[1 + 1.2\left(\frac{\tau_w}{\tau_c + \tau_w}\right)^{3.2}\right] \tag{7}$$

where τ_c and τ_w (N/m^2) are the bed shear stress due to currents and waves, respectively.

3. Results

Data sets of 19 semi-diurnal tides were recorded and were divided into two groups (Table 1). The first group was characterized by relatively high tides when tidal elevations in the tidal creek were higher than salt marsh elevation (i.e., 4.2 m), named over-marsh tides including T1, T3, T5, T7, and T9 during spring tide. The second group included the remaining tides when tidal elevations were lower than the salt marsh thus water motions were constrained within the tidal creeks, named creek-restricted tides.

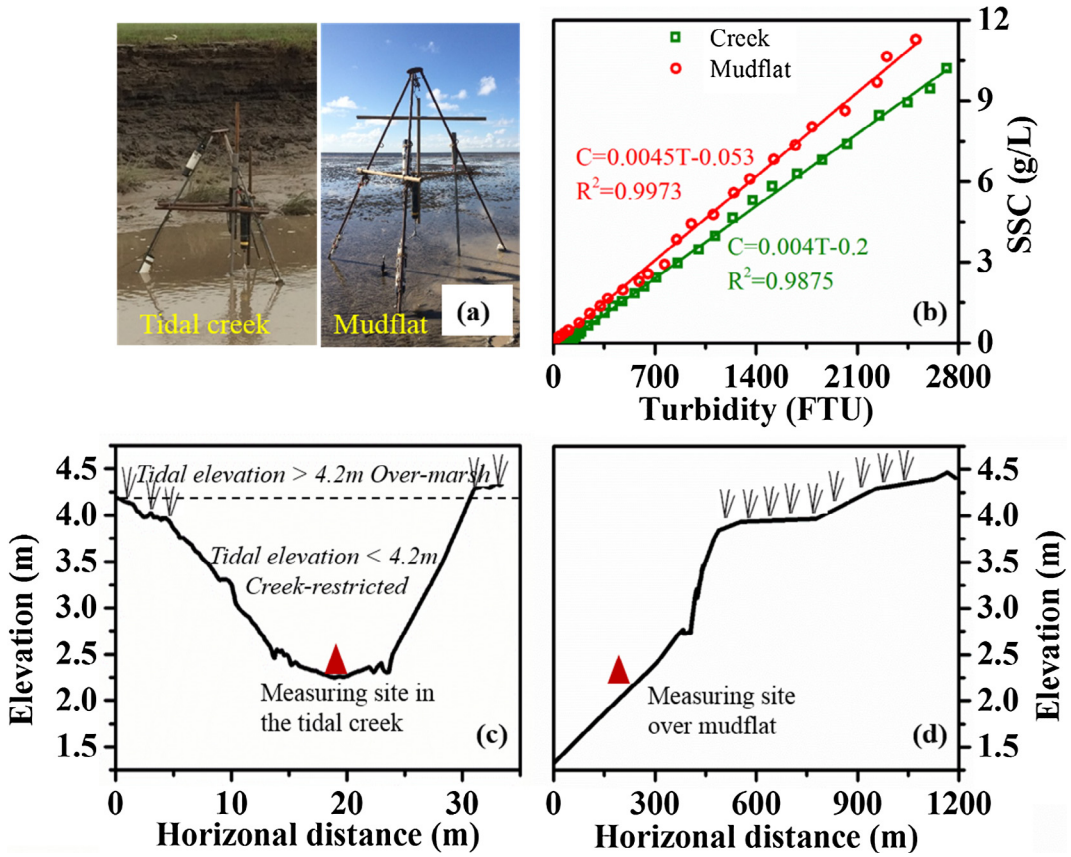

Fig. 2. (a) Measuring sites in the tidal creek (left) and the mudflat (right), (b) calibration of the optical backscatter signal with SSC data, (c) creek cross section, (d) location of the mudflat site.

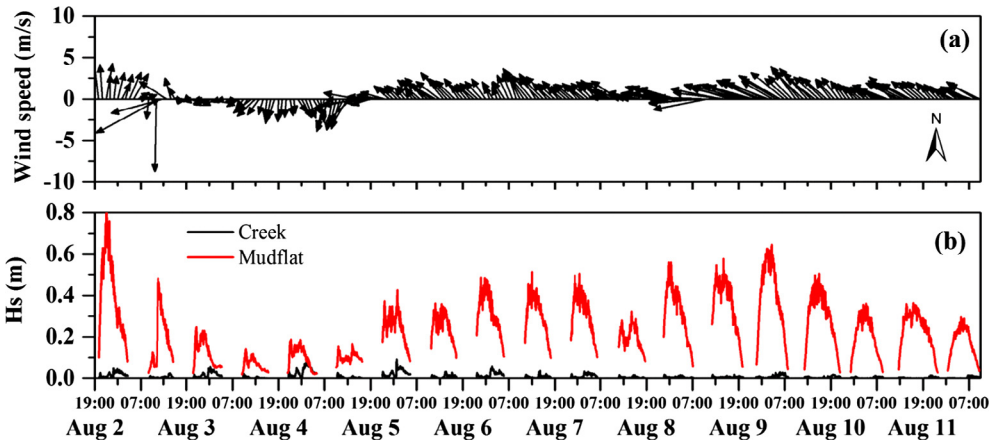

Fig. 3. (a) Hourly wind speeds recorded at the Eastern Chongming weather station, (b) time series of significant wave heights during the study period at the tidal creek site (red) and at the mudflat site (black). (For interpretation of the references to colour in this figure legend, the reader is referred to the web version of this article.)

3.1. Wind and waves

During the entire study period, the wind speed varied from ~0 to 9.7 m/s with an average value of 3.76 m/s, indicating that the observations were conducted under fair weather conditions. The winds were in onshore directions (120–180°) during most of the tides (T6 to T19), except for T1to T5 when the wind directions were alongshore (Fig. 3a).

At the mudflat site, the significant wave height (H_s) ranged from 0.02 to 0.83 m (Fig. 3b). The tidally averaged H_s of each tide ranged from 0.07 (T4) to 0.41 m (T1) and showed a positive correlation with wind speeds (Fig. 3). The averaged wave heights during neap tides (from T13 to T19) were generally greater than those during spring tides (from T1 to T7) due to the persistent landward winds during the field campain. However, there was no significant correlation between wave heights and water depth. At the tidal creek site, the RBR logger measured no wave activity during the deployment (wave height < 5 cm) (Fig. 3b).

3.2. Currents

The instantaneous current velocity ranged from 0.01 to 0.83 m/s at the tidal creek site and from 0.01 to 0.41 m/s at the mudflat site (Fig. 4b). Velocity measurements demonstrated that high tides (> 4.2 m, over-marsh tides) typically generated higher current velocities in the tidal creek (Fig. 5 and Table. 2). During T1, T3, T5, T7, and T9, the tidal mean current velocities (0.32–0.51 m/s; averagely, 0.44 m/s) were much higher than those during creek-restricted tides

Table 1
Summary of tidal conditions at the two study sites. The elevations are relative to the theoretical low-tide datum at Wusong.

Tides	Max. tidal elevation (m) (Referenced to datum at Wusong)		Over-marsh or creek-restricted
	Tidal creek (Site elevation: 2.2 m)	Mudflat (Site elevation: 2.1 m)	
T1	4.47	4.49	Over-marsh
T2	3.90	3.90	Creek-restricted
T3	4.55	4.57	Over-marsh
T4	3.99	3.99	Creek-restricted
T5	4.58	4.60	Over-marsh
T6	4.01	4.00	Creek-restricted
T7	4.46	4.47	Over-marsh
T8	3.92	3.91	Creek-restricted
T9	4.25	4.27	Over-marsh
T10	3.86	3.86	Creek-restricted
T11	4.08	4.08	Creek-restricted
T12	3.77	3.77	Creek-restricted
T13	3.93	3.99	Creek-restricted
T14	3.72	3.78	Creek-restricted
T15	3.64	3.70	Creek-restricted
T16	3.47	3.53	Creek-restricted
T17	3.28	3.35	Creek-restricted
T18	3.34	3.40	Creek-restricted
T19	2.91	2.97	Creek-restricted

(0.08–0.20 m/s; averagely, 0.15 m/s). While at the mudflat site, the higher mean current velocities still occurred during the over-marsh tides, however, the difference between over-marsh tides (0.22–0.27 m/s; averagely, 0.24 m/s) and creek-restricted tides (0.05–0.19 m/s; averagely, 0.14 m/s) was less significant (Table. 2).

Within tidal cycles, at the mudflat site, the current typically reached peak velocities during early flood and late ebb, both during over-marsh and creek-restricted tides. The time series of velocity displayed a strong similarity between the tidal creek site and the mudflat site during creek-restricted tides (Fig. 4b). By contrast, during over-marsh tides, besides early flood and late ebb, peak current velocities at the tidal creek site also occurred during late flood, when the creek was full and before flow flooded over the adjacent marsh (Fig. 4b).

3.3. Bed shear stress

3.3.1. Bed shear stress at the tidal creek site

The wave activities were weak at the tidal creek site and the bed shear stress was mainly controlled by currents (τ_c). The time series of τ_c are shown in Fig. 4d and the tidal mean τ_c ranged from 0.01 to 0.76 N/m^2 (Table. 2). On average, τ_c was greater during over-marsh tides (average, 0.37 N/m^2) than that during creek-restricted tides (average, 0.09 N/m^2). Within tidal cycles, peak τ_c occurred during late flood during high tides but no similar peak τ_c appeared during creek-restricted tides (Fig. 6).

3.3.2. Bed shear stress at the mudflat site

At the mudflat site, the bed shear stress was induced by both currents (τ_c) and waves (τ_w). The tidal mean τ_c ranged from 0.06 to 0.21 N/m^2 and τ_w ranged from 0.14 to 0.99 N/m^2 (Fig. 4c). The bed shear stress due to waves (τ_w) displayed a strong relationship with significant wave heights (Figs. 3b and 4c). The bed shear stress due to combined current-wave action (τ_{cw}) was calculated using a hydrodynamic model (Soulsby, 1995), and the results are shown in Fig. 4d and Table. 2. The tidal mean τ_{cw} ranged from 0.09 to 0.31 N/m^2 and τ_{cw} were significantly greater than τ_c (Figs. 4 and 6). On average, τ_{cw} during over-marsh tides (average, 0.18 N/m^2) was close to that during creek-restricted tides (average, 0.21 N/m^2).

3.4. Suspended sediment concentration

At the tidal creek site, the tidal mean suspended sediment concentration (SSC) ranged from 0.26 to 1.70 g/L and the peak SSCs occurred during early flood (Table. 2). The mean SSCs during over-marsh tides and creek-restricted tides were 0.90 and 1.13 g/L, respectively. While during over-marsh tides, besides early flood period, high values of SSC also were observed before the creek was filled. Then the SSC decreased after the tidal elevation exceeded the salt marsh elevation (Figs. 4e and 6). At the mudflat site, the tidal mean SSC ranged from 0.22 to 1.55 g/L (Table. 2). The mean SSCs during over-marsh tides and creek-restricted tides were 0.99 and 0.97 g/L, respectively. During creek-restricted tides, similar to the tidal creek site, the peak SSCs occurred during early flood (Fig. 6). However, during over-marsh tides, the SSC increased with the water depth and reached peak values before the slack water periods. After that, the SSC reduced markedly as the water depth decreased (Fig. 6).

3.5. Bed-level changes

At the tidal creek site, bed-level changes showed a significant trend towards erosion during over-marsh tides (Fig. 4f). The tidal creek was eroded by 35 mm between T1 and T9. However, during creek-restricted tides, the tidal creek switched to deposition and the elevation increased by 20 mm from T10 to T19 (Fig. 4f). While at the mudflat site, the bed-level changes were somewhat contrary compared to the tidal creek site, i.e., the mudflat was deposited by about 29 mm between T1 and T9 and eroded by 25 mm from T10 to T19 (Fig. 4f).

3.6. Sedimentary processes in the mudflat-creek system

During creek-restricted tides (T10–T19), low water depths combining with relatively high wind-induced wave activities, resulted in greater bed shear stresses and erosion at the mudflat site (Fig. 7). The resuspended sediments were transported landward to the salt marshes and the tidal creeks along with the flooding currents, leading to relatively high SSCs in these zones (Fig. 6d). On the other hand, the creek-restricted currents led to low velocities and low bed shear stresses in the tidal creeks, providing beneficial conditions for sediment settling and deposition therein (Figs. 4 and 6d). During over-marsh tides (T1, T3, T5, T7, and T9), fine-grained sediments in the adjacent estuarine area were resuspended and transported to the mudflats. Larger water depths, in combination with smaller bed shear stresses (Figs. 6e and 7), were favorable for deposition in the mudflats. In the meantime, over-marsh currents occurred in the tidal creek and led to lateral water and sediment spread to surrounding salt marshes (Fig. 5). The relatively large bed shear stress could lead to increase in the SSCs. The high SSCs, particularly when the currents were bankfull and flooded over the salt marshes, would lead to the deposition in the salt marshes, due to vegetation trapping and velocity decreasing (Fig. 6c).

We provided an integrated concept model described the sedimentary processes in intertidal environments based on the mudflat-creek system (Fig. 8). In this way, sedimentary processes in the study area could be inferred as: in a spring-neap tidal cycle, the sediments from the estuarine waters were transported to the mudflats and deposited during spring tides; afterwards, the sediments were resuspended from the mudflats and transported to tidal creeks during neap tides; when next spring tides came, the sediments in the tidal creeks are picked again and transported to the salt marshes and deposited therein through over-marsh currents.

4. Discussion

4.1. Role of mudflat-creek systems

Tide creeks and mudflats are both fundamental components in

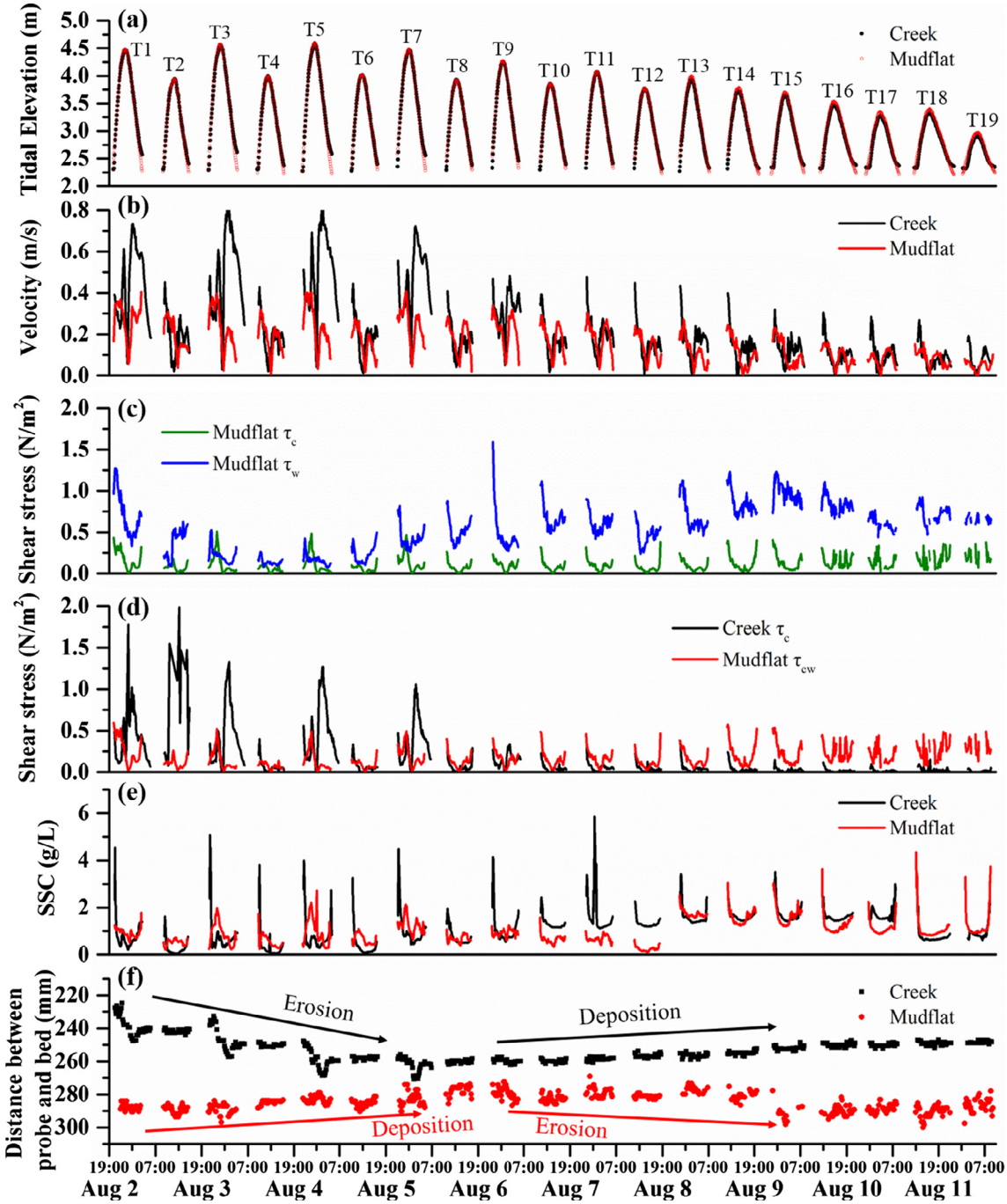

Fig. 4. Time series of (a) tidal elevations, (b) mean current velocity, (c) bed shear stress due to currents (τ_c) and waves (τ_w) at the mudflat site, (d) bed shear stress due to currents (τ_c) at the tidal creek site and bed shear stress due to the combined current-wave action (τ_{cw}) at the mudflat site, (e) SSC, (G) bed-level changes.

estuarine and coastal intertidal environments. A considerate amount of incoming suspended sediment from the adjacent riverine zone could be expected to deposit on the unvegetated mudflats (Whitehouse et al., 2000; Yang et al., 2005). Some of these sediments would be re-suspended and directly transported to the salt marshes, while some would be firstly delivered to the tidal creeks, then were spread and deposited over the salt marshes during over-marsh tides (Reed, 1989; Fagherazzi et al., 2012).

The measurements of simultaneous sedimentary processes on the salt marsh surface were lacking because we only conducted field measurements in the tidal creek and the mudflat. Therefore, we could not quantify the contributions of various sediment sources to deposition over salt marshes. However the sediments on the mudflats and in the tidal creeks have been considered as supply sources for the accretion of the intertidal environments, particularly for salt marshes (Stumpf, 1983; Temmerman et al., 2005b; Bouma et al., 2009; Mariotti et al., 2010; O'Laughlin and van Proosdij, 2013; Vandenbruwaene et al., 2015). Recent studies also indicated that short-term mudflat dynamics could drive long-term cyclic salt marsh dynamics (Bouma et al., 2016). Based on the sedimentary processes observed in the mudflat and in the creek, it is reasonable to infer the corresponding sedimentary processes on the marsh surface.

The results in this study indicated that there were spring-neap variations of erosion-deposition patterns, and sediment resource-sink shifts of mudflat-creek system. At neap tides, the eroded sediment at mudflats was transported towards tidal creeks and deposited therein,

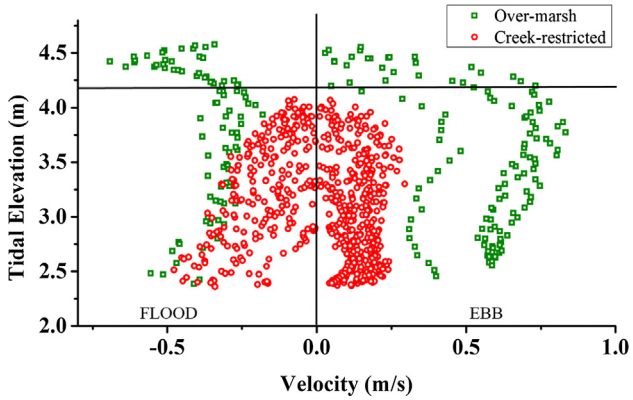

Fig. 5. Stage-velocity plot for the tidal creek site.

supplying sediment source for over-marsh deposition at spring tides. The accumulative effects of the spring-neap tidal variations of erosion-deposition within the mudflat-creek system were therefore responsible for sedimentary processes on the entire intertidal environment.

4.2. Controls of intertidal sedimentary processes

Under the combined effects of flat elevations, tidal currents, wind waves, and sediment supplies etc., an intertidal environment would reach a stable dynamic equilibrium, forming a mudflat-creek morphology (Temmerman et al., 2003; Friedrichs, 2011; Mariotti and Fagherazzi, 2013). Those equilibria are achieved through sediment exchange dynamic balances between current-dominated creeks and combined-wave-current-dominated mudflats (Shi et al., 2012; Mariotti and Fagherazzi, 2013).

The elevation of intertidal environment is important in intertidal sedimentary processes and dynamic equilibria, since the elevation exhibits a close relationship with the submerged time (Fagherazzi et al., 2012). In this study, during the studied spring-neap tidal cycle, the net changes in the elevation of the tidal creek site and the mudflat site are −15 mm and 4 mm, respectively. Erosions in the tidal creek would result in local lower water levels and relatively shorter over-marsh periods in the next tidal cycle. Thus more sediment tends to deposit in the tidal creek rather than over the salt marsh, leading to a recovery increase in the elevation of the tidal creek and a longer over-marsh period. In general, long over-marsh time is positively related to salt marsh depositions (Temmerman et al., 2003). The creek elevation is primarily controlled by tidal currents, including creek hydrodynamics and sediment transport. The tidal creek is eroded due to high bed shear stresses derived from currents (average, 0.37 N/m^2) during over-marsh tides whereas is deposited under low bed shear stresses (average, 0.09 N/m^2) at creek-restricted tides. Besides tidal currents, the mudflat elevation is also directly influenced by wave activities, which always results in high bed shear stresses and erosions in mudflats even at neap tides (Shi et al., 2017). The eroded sediments stemming from the combined effect of currents and waves in mudflats have significant influences on salt marsh depositions, through an intermediate bridge-tidal creek.

Field surveys based on terrestrial laser scanning data showed that the studied intertidal habitat accreted remarkably with abundant sediment supply during the study period (Xie et al., 2018). Previous studies have acknowledged the important role of sediment supply in intertidal sedimentary processes as well (Yang et al., 2005; Kirwan and Megonigal, 2013; Schuerch et al., 2014). Rich sediment supplies are positively linked to intertidal depositions, particularly for mudflats. This study emphasizes the significance of mudflat depositions as a sediment source for the mudflat-creek-marsh evolutions in particular. The sediment in mudflats is eroded, transported, and deposited within the mudflat-creek-marsh system, leading to a redistribution of sediment within the entire intertidal environment. The high sediment-loaded environment in the Yangtze Estuary provides enough sediment to maintain dynamic equilibria and accretions in intertidal environments (Yang et al., 2001). While in low sediment-loaded environments (e.g., Barnegat Bay), previous studies have reported that coastal intertidal environments generally experienced erosions (Leonardi et al., 2016).

4.3. Implications and limitations

Previous studies indicated that coastal management required a good understanding of sedimentary processes in intertidal environments, including mudflat dynamics, creek dynamics and salt marsh dynamics (Friedrichs, 2011; Zhu et al., 2012; Schuerch et al., 2014; Bouma et al., 2016). These physical processes were interactional rather than

Table 2
The results of the analysis of current velocity (m/s), bed shear stress (N/m^2), and suspended sediment concentration (SSC) (g/L) at the tidal creek site and mudflat site.

Tides	Velocity (m/s)						Bed shear stress (N/m^2)						SSC (g/L)					
	Tidal creek			Mudflat			Tidal creek (τ_c)			Mudflat (τ_{cw})			Tidal creek			Mudflat		
	Max	Min	Avg ± Std	Max	Min	Avg ± Std	Max	Min	Avg ± Std	Max	Min	Avg ± Std	Max	Min	Avg ± Std	Max	Min	Avg ± Std
1	0.74	0.06	0.43 ± 0.18	0.41	0.05	0.27 ± 0.09	1.78	0.06	0.42 ± 0.31	0.59	0.03	0.27 ± 0.17	4.54	0.21	0.82 ± 0.66	1.79	0.49	0.92 ± 0.21
2	0.45	0.02	0.19 ± 0.10	0.31	0.04	0.19 ± 0.07	1.99	0.08	0.76 ± 0.56	0.26	0.03	0.11 ± 0.05	1.63	0.03	0.26 ± 0.29	0.72	0.22	0.52 ± 0.13
3	0.83	0.03	0.49 ± 0.19	0.40	0.02	0.23 ± 0.10	1.33	0.00	0.43 ± 0.36	0.52	0.01	0.15 ± 0.12	5.08	0.28	0.79 ± 0.80	1.98	0.23	0.90 ± 0.47
4	0.43	0.02	0.18 ± 0.09	0.32	0.01	0.19 ± 0.07	0.40	0.00	0.06 ± 0.07	0.14	0.01	0.08 ± 0.04	3.80	0.06	0.33 ± 0.60	1.03	0.25	0.54 ± 0.23
5	0.81	0.04	0.51 ± 0.18	0.41	0.03	0.24 ± 0.11	1.27	0.00	0.48 ± 0.35	0.49	0.01	0.14 ± 0.12	4.00	0.29	0.77 ± 0.70	2.22	0.28	1.00 ± 0.58
6	0.44	0.01	0.19 ± 0.10	0.28	0.02	0.16 ± 0.07	0.33	0.00	0.06 ± 0.06	0.26	0.01	0.09 ± 0.05	3.27	0.06	0.35 ± 0.50	1.09	0.38	0.64 ± 0.23
7	0.72	0.06	0.47 ± 0.15	0.41	0.04	0.24 ± 0.09	1.06	0.00	0.39 ± 0.27	0.49	0.02	0.19 ± 0.12	4.48	0.43	1.06 ± 0.81	2.13	0.68	1.25 ± 0.34
8	0.41	0.04	0.18 ± 0.08	0.29	0.02	0.18 ± 0.07	0.29	0.00	0.06 ± 0.06	0.40	0.02	0.13 ± 0.08	1.95	0.49	0.72 ± 0.34	1.08	0.42	0.69 ± 0.15
9	0.48	0.05	0.32 ± 0.09	0.34	0.05	0.22 ± 0.08	0.34	0.00	0.15 ± 0.08	0.41	0.02	0.16 ± 0.08	4.15	0.54	1.02 ± 0.63	1.21	0.60	0.92 ± 0.14
10	0.39	0.02	0.17 ± 0.09	0.29	0.04	0.18 ± 0.07	0.23	0.00	0.04 ± 0.04	0.48	0.03	0.15 ± 0.11	2.44	1.16	1.32 ± 0.26	1.01	0.33	0.63 ± 0.13
11	0.48	0.05	0.20 ± 0.08	0.31	0.03	0.18 ± 0.07	0.30	0.00	0.06 ± 0.05	0.46	0.03	0.16 ± 0.08	5.87	1.13	1.70 ± 0.96	0.96	0.37	0.67 ± 0.13
12	0.45	0.01	0.16 ± 0.08	0.24	0.03	0.14 ± 0.06	0.22	0.00	0.05 ± 0.05	0.47	0.02	0.11 ± 0.08	2.25	1.20	1.32 ± 0.20	0.58	0.11	0.25 ± 0.10
13	0.44	0.01	0.17 ± 0.08	0.27	0.01	0.12 ± 0.07	0.37	0.00	0.05 ± 0.06	0.38	0.04	0.16 ± 0.09	3.43	1.35	1.60 ± 0.42	2.52	1.55	1.74 ± 0.18
14	0.40	0.00	0.14 ± 0.08	0.25	0.01	0.11 ± 0.07	0.24	0.00	0.04 ± 0.05	0.57	0.06	0.20 ± 0.14	2.50	1.44	1.60 ± 0.18	3.05	1.23	1.59 ± 0.34
15	0.32	0.02	0.13 ± 0.06	0.23	0.03	0.11 ± 0.07	0.15	0.00	0.03 ± 0.02	0.53	0.08	0.22 ± 0.14	3.50	1.41	1.69 ± 0.37	3.04	1.21	1.68 ± 0.45
16	0.31	0.01	0.11 ± 0.06	0.16	0.01	0.09 ± 0.04	0.12	0.00	0.02 ± 0.02	0.45	0.11	0.24 ± 0.10	2.46	1.44	1.58 ± 0.14	3.63	0.95	1.25 ± 0.42
17	0.29	0.01	0.10 ± 0.06	0.14	0.00	0.08 ± 0.04	0.09	0.00	0.02 ± 0.02	0.44	0.05	0.20 ± 0.09	3.00	1.40	1.70 ± 0.31	2.25	0.90	1.13 ± 0.29
18	0.27	0.01	0.09 ± 0.05	0.16	0.00	0.08 ± 0.04	0.15	0.00	0.03 ± 0.03	0.49	0.07	0.26 ± 0.11	2.07	0.61	0.72 ± 0.20	3.20	0.82	1.04 ± 0.43
19	0.19	0.01	0.08 ± 0.05	0.10	0.00	0.05 ± 0.02	0.05	0.00	0.01 ± 0.01	0.50	0.13	0.31 ± 0.09	2.41	0.61	0.92 ± 0.30	3.30	0.93	1.22 ± 0.55

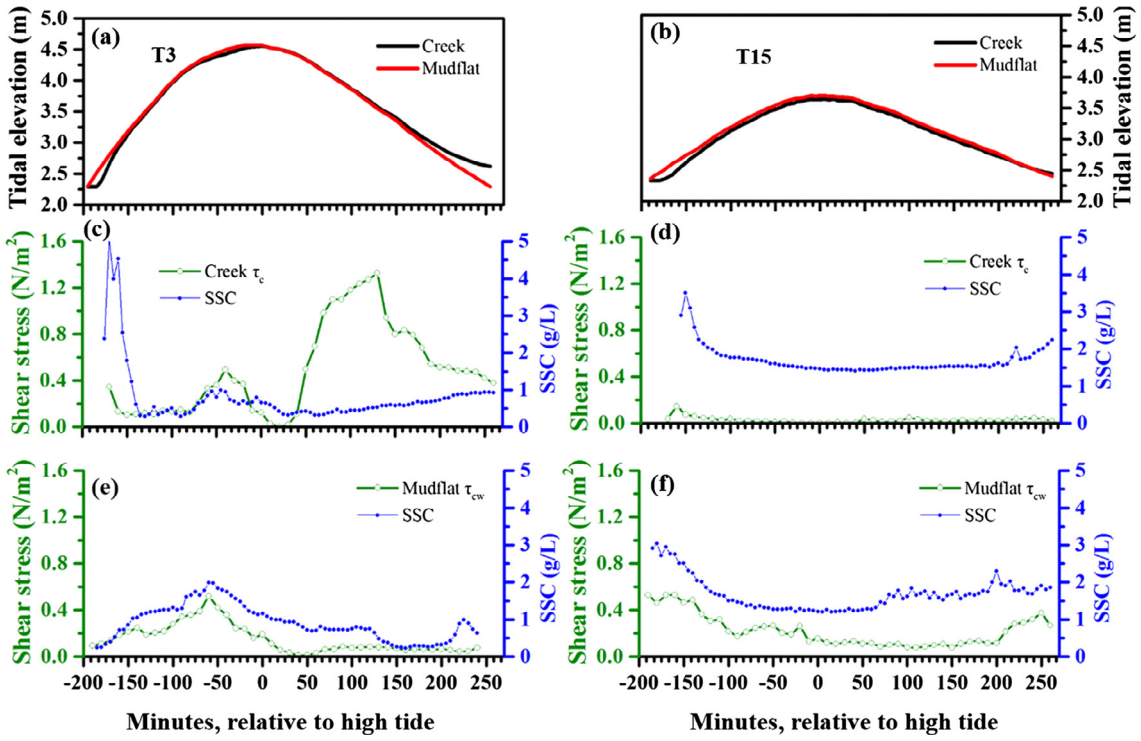

Fig. 6. Representative time-series of over-marsh (a, c, e) (e.g. tide 3) and creek-restricted (b, d, f) (e.g. tide 15) tides. The relationship between SSC and bed shear stress are displayed: (c) the tidal creek site during over-marsh tides, (d) the tidal creek site during creek-restricted tides, (e) the mudflat site during over-marsh tides, (f) the mudflat site during creek-restricted tides.

independent. The current study suggested that physical processes over salt marshes were linked to those in mudflats by tidal creeks. The mudflats served as a provisional sediment 'sink' with respect to much large scale estuarine and coastal waters while on the other hand as a sediment 'source' of tidal creeks. Tidal creeks formed as 'blood tubes' received sediment from seaward mudflats and then transported them to adjacent salt marshes, thus could be seen as a 'sink' of mudflat sediment and a sediment 'source' of salt marsh deposition. The mudflat-creek systems establish coherent links in sediment exchanges between intertidal environments and oceans.

Moreover, it should be noted that the above sedimentary patterns of the mudflat-creek system were valid under fair weather conditions. The erosion-deposition patterns might be quite different under storms regarding more elevated water level and much stronger wave influences (Leonardi and Fagherazzi, 2015). Severe erosion was highly likely to occur in the mudflat during storms because of much larger great τ_{cw} (Yang et al., 2003; Mariotti et al., 2010). These eroded sediments would end in mudflat-creek systems and finally deposited in salt marshes (Yang et al., 2003; Xie et al., 2017). It remains unknown it is the small but persisting evolution driven by tides under fair weather or the episodic but strong changes induced by waves play a more important role on longer term intertidal morphodynamics.

Although the tidal creeks were important for the sedimentary processes in the salt marshes, particularly for the high-elevation zonation (Allen, 2000; Christiansen et al., 2000; Friedrichs, 2011; Fagherazzi et al., 2012), marsh edge erosion and retreat and subsequent landward sediment transport would also stimulate salt marsh accretion (Temmerman et al., 2013; Bouma et al., 2016). Previous studies showed that in macro-tidal estuaries and coasts, a considerate portion of the total marsh sedimentation was attributed to landward sediment transport from mudflat directly (crossing marsh edges) (Davidson-Arnott et al., 2002; van Proosdij et al., 2006). The proportion of total sediment input from marsh edges displayed a positive relationship with the tidal elevation (or water depth) (Temmerman et al., 2005a). There were

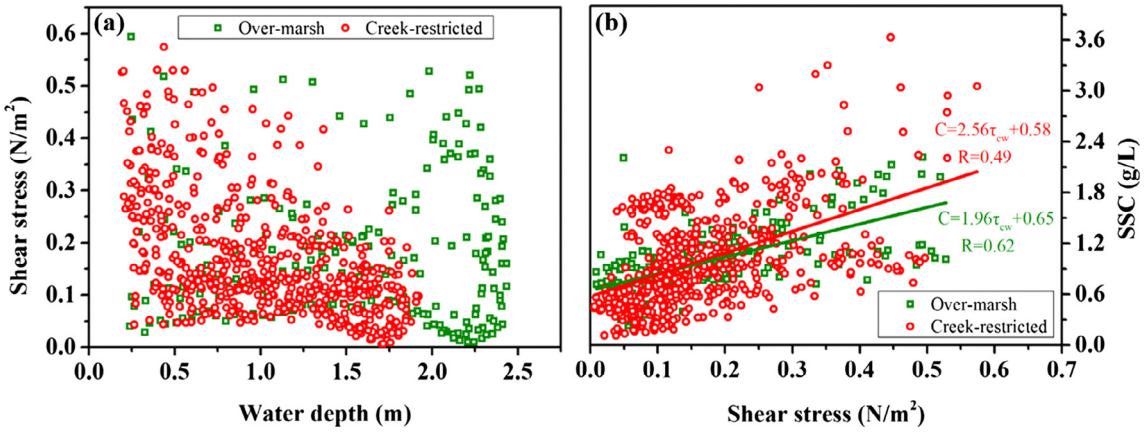

Fig. 7. At the mudflat site, (a) scatterplots relating bed shear stress to water depth, (b) scatterplots relating SSC to bed shear stress.

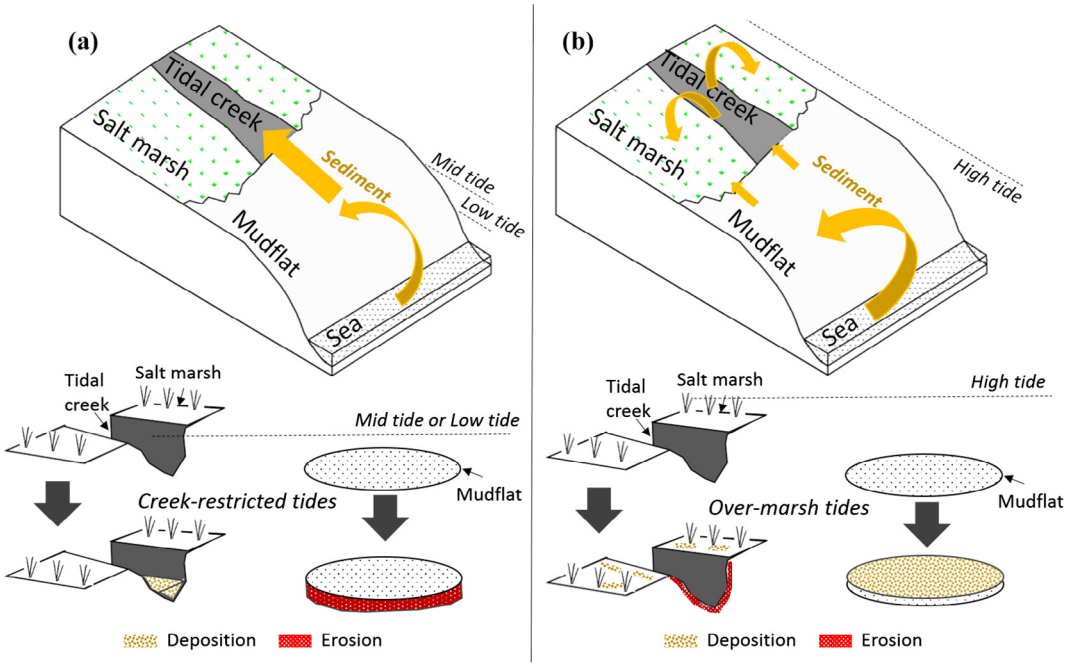

Fig. 8. Conceptual model for the sedimentary process in the intertidal environments of the Yangtze Delta under fair weather conditions, based on the mudflat-creek system. (a) during low tides (neap tides) and (b) high tides (spring tides).

evidences that the salt marsh edges were eroded apparently during storms and the sediments would deposit near mudflats in the Yangtze Estuary (Xie et al., 2018). These freshly deposited sediments thus could provide extra sources to be transported into tidal creeks and salt marshes. Further work is needed to consider the sediment transport linking mudflat-marsh and mudflat-creek-marsh.

5. Conclusions

This paper investigated the role of mudflat-creek exchanges in sedimentary processes over an intertidal habitat in the Yangtze Estuary. We conducted field measurements of water levels, waves, velocities, SSCs, and bed-level changes in a tidal creek and its adjacent mudflat. During high tides, the bed shear stress (average, 0.18 N/m^2) was low in the mudflats. Meanwhile, SSC (average, 0.99 g/L) was high due to large amounts of sediment input from large scale estuarine waters, leading to deposition and an elevation increase of 29 mm in the mudflats. In the meantime, sediment in the tidal creek was resuspended by the relatively high bed shear stress (average, 0.37 N/m^2), and deposited over the salt marsh during over-marsh periods. The elevation of the tidal creek decreased by 35 mm. By contrary, during low tides, the water depth was low and the bed shear stress (average, 0.21 N/m^2) was relatively high in the mudflats, which resulted in sediment resuspension (average SSC, 0.97 g/L) and an elevation decrease of 25 mm. The resuspended sediment was delivered to the tidal creek and deposited due to the low bed shear stress (average, 0.09 N/m^2). The elevation of the tidal creek increased by 20 mm.

This study generalizes a unified concept model to describe the sedimentary processes in intertidal environments based on a sediment transport conduit in the mudflat-creek systems. The sediments from the estuarine waters are transported to the mudflats and deposited during flood tides. Afterwards, the sediments are resuspended from the mudflats and transported to tidal creeks during neap tides. When next over-marsh tides come, the sediments in the tidal creeks are flushed over the salt marshes and deposit through over-marsh currents.

The results indicate that there is an erosion-deposition cycle in the mudflat-creek system during a spring-neap tidal cycle under fair weather conditions, which further influences the morphodynamics over the salt marsh and sedimentary processes in intertidal environments. These findings likely represent the morphological configuration of most intertidal environments. Further studies are required to better understand the effect of sediment fluxes across marsh edges on intertidal evolutions. Additional impact factors may also worth further investigation.

6. Declarations of interest

None.

Acknowledgments

This study was supported by the National Natural Science Foundation of China (Nos. 51739005, 51320105005, 41406094, 41506105, 41876091). Financial support from the Shanghai Science and Technology Committee (No. 17DZ1204800) are also acknowledged. Leicheng Guo is supported by China Post-Doc fund (No. 2016T90351). We would like to thank Chao Guo, Jianliang Lin, Siming Chen, and Menghan Wang for their assistance in the field work. The authors are also grateful to two anonymous reviewer for their constructive comments to greatly improve this manuscript. We also thank Prof. Geoff Syme, Editor-in-Chief, for granting us the opportunity to submit a revised manuscript.

References

Allen, J.R.L., 2000. Morphodynamics of Holocene salt marshes: a review sketch from the Atlantic and Southern North Sea coasts of Europe. Quat. Sci. Rev. 19 (12), 1155–1231.

Andersen, T.J., Fredsoe, J., Pejrup, M., 2007. In situ estimation of erosion and deposition thresholds by Acoustic Doppler Velocimeter (ADV). Estuar. Coast. Shelf Sci. 75 (3), 327–336.

Bouma, T.J., Friedrichs, M., van Wesenbeeck, B.K., Temmerman, S., Graf, G., Herman, P.M.J., 2009. Density-dependent linkage of scale-dependent feedbacks: a flume study on the intertidal macrophyteSpartina anglica. Oikos 118 (2), 260–268.

Bouma, T.J., van Belzen, J., Balke, T., van Dalen, J., Klaassen, P., Hartog, A.M., Callaghan, D.P., Hu, Z., Stive, M.J.F., Temmerman, S., Herman, P.M.J., 2016. Short-term mudflat dynamics drive long-term cyclic salt marsh dynamics. Limnol. Oceanogr. 61 (6), 2261–2275.

Christiansen, T., Wiberg, P.L., Milligan, T.G., 2000. Flow and sediment transport on a tidal salt marsh surface. Estuar. Coast. Shelf Sci. 50 (3), 315–331.

D'Alpaos, A., Lanzoni, S., Marani, M., Rinaldo, A., 2007. Landscape evolution in tidal embayments: modeling the interplay of erosion, sedimentation, and vegetation dynamics. J. Geophys. Res. 112 (F1), 1–17.
Davidson-Arnott, R.G.D., van Proosdij, D., Ollerhead, J., Schostak, L., 2002. Hydrodynamics and sedimentation in salt marshes: examples from a macrotidal marsh. Bay of Fundy. Geomorphology 48 (1–3), 209–231.
Dronkers, J., 1986. Tidal asymmetry and estuarine morphology. Neth. J. Sea Res. 20 (2), 117–131.
Dyer, K.R., Christie, M.C., Feates, N., Fennessy, M.J., Pejrup, M., van der Lee, W., 2000. An investigation into processes influencing the morphodynamics of an intertidal mudflat, the dollard estuary, The Netherlands: I. Hydrodynamics and suspended sediment. Estuar. Coast. Shelf Sci. 50 (5), 607–625.
Eaton, T.T., 2016. Tidal reversal and flow velocities using temperature and specific conductance in a small wetland creek. J. Hydrol. 542, 552–563.
Eisma, D., 1998. Intertidal Deposits: River Mouths, Tidal Flats, and Coastal Lagoons. CRC Press, Boca Raton, Florida, pp. 459.
Fagherazzi, S., Wiberg, P.L., 2009. Importance of wind conditions, fetch, and water levels on wave-generated shear stresses in shallow intertidal basins. J. Geophys. Res. 114 (F3), 1–12.
Fagherazzi, S., Kirwan, M.L., Mudd, S.M., Guntenspergen, G.R., Temmerman, S., D'Alpaos, A., van de Koppel, J., Rybczyk, J.M., Reyes, E., Craft, C., Clough, J., 2012. Numerical models of salt marsh evolution: ecological, geomorphic, and climatic factors. Rev. Geophys. 50 (1), 1–28.
Friedrichs, C.T., 2011. Tidal flat morphodynamics: a synthesis. In: Wolanski, E., McLusky, D. (Eds.), Treatise on Estuarine and Coastal Science, 137–170.
Gedan, K.B., Kirwan, M.L., Wolanski, E., Barbier, E.B., Silliman, B.R., 2011. The present and future role of coastal wetland vegetation in protecting shorelines: answering recent challenges to the paradigm. Clim. Change 106 (1), 7–29.
Howes, N.C., FitzGerald, D.M., Hughes, Z.J., Georgiou, I.Y., Kulp, M.A., Miner, M.D., Smith, J.M., Barras, J.A., 2010. Hurricane-induced failure of low salinity wetlands. Proc. Natl. Acad. Sci. 107 (32), 14014–14019.
Hu, Z., Wang, Z.B., Zitman, T.J., Stive, M.J.F., Bouma, T.J., 2015. Predicting long-term and short-term tidal flat morphodynamics using a dynamic equilibrium theory. J. Geophys. Res. Earth Surf. 120 (9), 1803–1823.
Hunt, S., Bryan, K.R., Mullarney, J.C., 2015. The influence of wind and waves on the existence of stable intertidal morphology in meso-tidal estuaries. Geomorphology 228, 158–174.
Janssen-Stelder, B., 2000. The effect of different hydrodynamic conditions on the morphodynamics of a tidal mudflat in the Dutch Wadden Sea. Cont. Shelf Res. 20 (12–13), 1461–1478.
Kim, S.C., Friedrichs, C.T., Maa, P.Y., Wright, L.D., 2000. Estimating bottom stress in tidal boundary layer from acoustic Doppler velocimeter data. J. Hydraul. Eng. 126 (6), 399–406.
Kirwan, M.L., Megonigal, J.P., 2013. Tidal wetland stability in the face of human impacts and sea-level rise. Nature 504 (7478), 53–60.
Leonardi, N., Defne, Z., Ganju, N.K., Fagherazzi, S., 2016. Salt marsh erosion rates and boundary features in a shallow Bay. J. Geophys. Res. Earth Surf. 121 (10), 1861–1875.
Leonardi, N., Fagherazzi, S., 2015. Effect of local variability in erosional resistance on large-scale morphodynamic response of salt marshes to wind waves and extreme events. Geophys. Res. Lett. 42 (14), 5872–5879.
Li, X., Zhou, Y., Zhang, L., Kuang, R., 2014. Shoreline change of Chongming Dongtan and response to river sediment load: a remote sensing assessment. J. Hydrol. 511, 432–442.
Luan, H.L., Ding, P.X., Wang, Z.B., Ge, J.Z., Yang, S.L., 2016. Decadal morphological evolution of the Yangtze Estuary in response to river input changes and estuarine engineering projects. Geomorphology 256, 12–23.
Mariotti, G., Fagherazzi, S., 2013. A two-point dynamic model for the coupled evolution of channels and tidal flats. J. Geophys. Res. Earth Surf. 118 (3), 1387–1399.
Mariotti, G., Fagherazzi, S., Wiberg, P.L., McGlathery, K.J., Carniello, L., Defina, A., 2010. Influence of storm surges and sea level on shallow tidal basin erosive processes. J. Geophys. Res. 115 (C11), 0148–0227.
Moller, I., Spencer, T., French, J.R., Leggett, D.J., Dixon, M., 1999. Wave transformation over salt marshes: a field and numerical modelling study from North Norfolk, England. Estuar. Coast. Shelf Sci. 49 (3), 411–426.
Nyman, J.A., La Peyre, M.K., Caldwell, A., Piazza, S., Thom, C., Winslow, C., 2009. Defining restoration targets for water depth and salinity in wind-dominated Spartina patens (Ait.) Muhl. coastal marshes. J. Hydrol. 376 (3–4), 327–336.
O'Laughlin, C., van Proosdij, D., 2013. Influence of varying tidal prism on hydrodynamics and sedimentary processes in a hypertidal salt marsh creek. Earth Surf. Proc. Land. 38 (5), 534–546.
Pope, N.D., Widdows, J., Brinsley, M.D., 2006. Estimation of bed shear stress using the turbulent kinetic energy approach—A comparison of annular flume and field data. Cont. Shelf Res. 26 (8), 959–970.
Postma, H., 1961. Transport and accumulation of suspended matter in the Dutch Wadden Sea. Neth. J. Sea Res. 1 (1–2), 148–180.
Reed, D.J., 1989. Patterns of sediment deposition in subsiding coastal salt marshes, Terrebonne Bay, Louisiana: the role of winter storms. Estuaries 12 (4), 222–227.
Rijn, L.C.V., 1993. Principles of Sediment Transport in Rivers, Estuaries and Coastal Seas. Aqua Publications, Amsterdam, The Netherlands.
Salehi, M., Strom, K., 2012. Measurement of critical shear stress for mud mixtures in the San Jacinto estuary under different wave and current combinations. Cont. Shelf Res. 47, 78–92.
Schuerch, M., Dolch, T., Reise, K., Vafeidis, A.T., 2014. Unravelling interactions between salt marsh evolution and sedimentary processes in the Wadden Sea (southeastern North Sea). Prog. Phys. Geogr. 38 (6), 691–715.
Shi, B.W., Yang, S.L., Wang, Y.P., Bouma, T.J., Zhu, Q., 2012. Relating accretion and erosion at an exposed tidal wetland to the bottom shear stress of combined current–wave action. Geomorphology 138 (1), 380–389.
Shi, B.W., Yang, S.L., Wang, Y.P., Li, G.C., Li, M.L., Li, P., Li, C., 2017. Role of wind in erosion-accretion cycles on an estuarine mudflat. J. Geophys. Res. Oceans 122, 193–206.
Soulsby, R., 1997. Dynamics of marine sands. A manual for practical applications. Thomas Telford.
Soulsby, R.L., 1995. Bed Shear-Stress due to Combined Waves and Currents Advances in Coastal Morphodynamics. Delft Hydraulics, The Netherlands, pp. 4–23.
Stapleton, K.R., Huntley, D.A., 1995. Seabed stress determinations using the inertial dissipation method and the turbulent kinetic energy method. Earth Surf. Proc. Land. 20 (9), 807–815.
Stumpf, R.P., 1983. The process of sedimentation on the surface of a salt marsh. Estuar. Coast. Shelf Sci. 17 (5), 495–508.
Temmerman, S., Bouma, T.J., Govers, G., Lauwaet, D., 2005a. Flow paths of water and sediment in a tidal marsh: relations with marsh developmental stage and tidal inundation height. Estuaries 28 (3), 338–352.
Temmerman, S., Bouma, T.J., Govers, G., Wang, Z.B., De Vries, M.B., Herman, P.M.J., 2005b. Impact of vegetation on flow routing and sedimentation patterns: three-dimensional modeling for a tidal marsh. J. Geophys. Res. Earth Surf. 110 (F4), 1–18.
Temmerman, S., Bouma, T.J., Van de Koppel, J., Van der Wal, D., De Vries, M.B., Herman, P., 2007. Vegetation causes channel erosion in a tidal landscape. Geology 35 (7), 631–634.
Temmerman, S., Govers, G., Wartel, S., Meire, P., 2003. Spatial and temporal factors controlling short-term sedimentation in a salt and freshwater tidal marsh, Scheldt estuary, Belgium, SW Netherlands. Earth Surf. Proc. Land. 28 (7), 739–755.
Temmerman, S., Meire, P., Bouma, T.J., Herman, P., Ysebaert, T., 2013. Ecosystem-based coastal defence in the face of global change. Nature 504, 79–83.
Tian, B., Zhou, Y., Thom, R.M., Diefenderfer, H.L., Yuan, Q., 2015. Detecting wetland changes in Shanghai, China using FORMOSAT and Landsat TM imagery. J. Hydrol. 529, 1–10.
Tian, B., Zhou, Y., Zhang, L., Yuan, L., 2008. Analyzing the habitat suitability for migratory birds at the Chongming Dongtan Nature Reserve in Shanghai, China. Estuar. Coast. Shelf Sci. 80 (2), 296–302.
van der Wegen, M., Jaffe, B., Foxgrover, A., Roelvink, D., 2017. Mudflat morphodynamics and the impact of sea level rise in South San Francisco Bay. Estuaries Coasts 40 (1), 37–49.
van Maren, D.S., Yang, S., He, Q., 2013. The impact of silt trapping in large reservoirs on downstream morphology: the Yangtze River. Ocean Dyn. 63 (6), 691–707.
van Proosdij, D., Ollerhead, J., Davidson-Arnott, R.G.D., 2006. Seasonal and annual variations in the volumetric sediment balance of a macro-tidal salt marsh. Mar. Geol. 225 (1–4), 103–127.
Vandenbruwaene, W., Schwarz, C., Bouma, T.J., Meire, P., Temmerman, S., 2015. Landscape-scale flow patterns over a vegetated tidal marsh and an unvegetated tidal flat: implications for the landform properties of the intertidal floodplain. Geomorphology 231, 40–52.
Voulgaris, G., Meyers, S.T., 2004. Temporal variability of hydrodynamics, sediment concentration and sediment settling velocity in a tidal creek. Cont. Shelf Res. 24 (15), 1659–1683.
Wang, Z.B., Jeuken, M.C.J.L., Gerritsen, H., Vriend, H.J.D., Kornman, B.A., 2002. Morphology and asymmetry of the vertical tide in the Westerschelde estuary. Cont. Shelf Res. 22 (17), 2599–2609.
Wang, J., Du, J., Baskaran, M., Zhang, J., 2016. Mobile mud dynamics in the East China Sea elucidated using 210Pb, 137Cs, 7Be, and 234Th as tracers. J. Geophys. Res. Oceans 121, 224–239.
Whitehouse, R., Bassoullet, P., Dyer, K.R., Mitchener, H.J., Roberts, W., 2000. The influence of bedforms on flow and sediment transport over intertidal mudflats. Cont. Shelf Res. 20 (10), 1099–1124.
Widdows, J., Pope, N.D., Brinsley, M.D., 2008. Effect of Spartina anglica stems on near-bed hydrodynamics, sediment erodability and morphological changes on an intertidal mudflat. Mar. Ecol. Prog. Ser. 362, 45–57.
Xie, W., He, Q., Zhang, K., Guo, L., Wang, X., Shen, J., Cui, Z., 2017. Application of terrestrial laser scanner on tidal flat morphology at a typhoon event timescale. Geomorphology 292, 47–58.
Xie, W., He, Q., Zhang, K., Guo, L., Wang, X., Shen, J., 2018. Impacts of human modifications and natural variations on short-term morphological changes in estuarine tidal flats. Estuaries Coasts 42 (5), 1253–1267.
Xin, P., Kong, J., Li, L., Barry, D.A., 2012. Effects of soil stratigraphy on pore-water flow in a creek-marsh system. J. Hydrol. 475, 175–187.
Yang, S., Ding, P., Chen, S., 2001. Changes in progradation rate of the tidal flats at the mouth of the Changjiang (Yangtze) River, China. Geomorphology 38 (1–2), 167–180.
Yang, S.L., Friedrichs, C.T., Shi, Z., Ding, P.X., Zhu, J., Zhao, Q.Y., 2003. Morphological response of tidal marshes, flats and channels of the outer Yangtze River mouth to a major storm. Estuaries 26 (6), 1416–1425.
Yang, S.L., Li, H., Ysebaert, T., Bouma, T.J., Zhang, W.X., Wang, Y.Y., Li, P., Li, M., Ding, P.X., 2008. Spatial and temporal variations in sediment grain size in tidal wetlands, Yangtze Delta: on the role of physical and biotic controls. Estuar. Coast. Shelf Sci. 77 (4), 657–671.
Yang, S.L., Zhang, J., Zhu, J., Smith, J.P., Dai, S.B., Gao, A., Li, P., 2005. Impact of dams on Yangtze River sediment supply to the sea and delta intertidal wetland response. J. Geophys. Res. Earth Surf. 110 (F3), 247–275.
Ysebaert, T., Herman, P.M.J., Meire, P., Craeymeersch, J., Verbeek, H., Heip, C.H.R., 2003. Large-scale spatial patterns in estuaries: estuarine macrobenthic communities in the Schelde estuary, NW Europe. Estuar. Coast. Shelf Sci. 57 (1–2), 335–355.
Zhu, Q., van Prooijen, B.C., Wang, Z.B., Ma, Y.X., Yang, S.L., 2016. Bed shear stress estimation on an open intertidal flat using in situ measurements. Estuar. Coast. Shelf Sci. 182, 190–201.
Zhu, Q., Yang, S., Ma, Y., 2014. Intra-tidal sedimentary processes associated with combined wave–current action on an exposed, erosional mudflat, southeastern Yangtze River Delta, China. Mar. Geol. 347, 95–106.
Zhu, Z., Zhang, L., Wang, N., Schwarz, C., Ysebaert, T., 2012. Interactions between the range expansion of saltmarsh vegetation and hydrodynamic regimes in the Yangtze Estuary, China. Estuar. Coast. Shelf Sci. 96 (1), 273–279.